

Interactions of spatial solitons with fused couplers

Alon Harel and Boris A. Malomed

Department of Physical Electronics, School of Electrical Engineering, Faculty of Engineering, Tel Aviv University, Tel Aviv 69978, Israel

(Received 8 January 2014; published 7 April 2014)

We study dynamical and stationary states of solitons in dual-core waveguides which are locally coupled (*fused*) at one or several short segments. The model applies to planar optical waveguides, and to Bose-Einstein condensate in dual traps. Collisions of an incident soliton with single and double locally fused couplers are investigated by means of systematic simulations and several analytical methods (quasilinear, fast-soliton, and adiabatic approximations). Excitation dynamics of a soliton trapped by a local coupler is studied by means of the variational approximation, and verified by simulations. Shuttle motion of a soliton trapped in a cavity between two local couplers, and in a finite array of couplers, is studied too.

DOI: [10.1103/PhysRevA.89.043809](https://doi.org/10.1103/PhysRevA.89.043809)

PACS number(s): 42.65.Tg, 05.45.Yv, 42.65.Wi, 03.75.Lm

I. INTRODUCTION

One of basic types of optical waveguides is represented by dual-core couplers, in which parallel guiding cores interact via evanescent fields [1]. If the intrinsic nonlinearity in the cores is strong enough, the power exchange between them is affected by the intensity of the guided signals [2], which is a basis for the design of all-optical switching devices [3–5] and other applications, such as nonlinear amplifiers [6], stabilization of WDM (wavelength-division-multiplexed) transmission schemes [7], and logic gates [8]. In addition to the simplest dual-core system, realizations of nonlinear couplers have been proposed in many other settings, including the use of orthogonal polarizations of light [9]; semiconductor waveguides [10]; twin-core Bragg gratings [11,12]; systems with saturable [13], quadratic [14,15], and cubic-quintic (CQ) [16] nonlinearities; plasmonic media [17], dual-core traps for matter waves in Bose-Einstein condensates (BEC) [18,19], parallel arrays of discrete waveguides [20], nonlocal intracore nonlinearity [21], couplers for spatiotemporal “light bullets” in dual-core planar waveguides [22], and \mathcal{PT} -symmetric nonlinear couplers [23].

A fundamental property of nonlinear couplers with symmetric cores is the *symmetry-breaking bifurcation* (SBB), which destabilizes obvious symmetric modes and gives rise to asymmetric ones. The SBB was analyzed, at first, for spatially uniform states [24], and then for solitons in twin-core regular waveguides [25–28] and Bragg gratings [11] with the Kerr (cubic) nonlinearity (see also an early review [29], and a more advanced one [30]). The SBB analysis was then extended to solitons in couplers with the quadratic [14] and CQ [16] nonlinearities.

The Kerr nonlinearity in the dual-core system gives rise to the *subcritical* SBB for solitons, with originally unstable branches of emerging asymmetric modes going backward (to weaker nonlinearity) and then turning forward [31]. The asymmetric modes retrieve the stability at the turning points. On the other hand, the *supercritical* SBB gives rise to stable branches of asymmetric solitons going in the forward direction. The SBB of the latter type occurs in twin-core Bragg grating [11], and in the case of the quadratic nonlinearity [14]. The system with the CQ nonlinearity gives rise to a *bifurcation loop*, whose shape may be concave or convex [16].

Along with to the numerical analysis of soliton modes in nonlinear dual-core systems, the SBB point was found in an exact analytical form for the system with the cubic nonlinearity [25], and the emerging asymmetric modes were studied by means of the variational approximation (VA) (see original works [4,11,13,14,22,26] and review [30]).

In addition to the studies of solitons in uniform dual-core systems, analysis was also developed for *fused couplers*, in which the two cores are joined in a narrow segment [32]. In the simplest approximation, the corresponding dependence of the coupling strength on transverse coordinate x may be approximated by the delta function, $\delta(x)$. In previous works, interactions of solitons with such a locally fused segment were studied in the temporal domain, viz., for bright [32,33] and dark [34] solitons in dual-core optical fibers and fiber lasers [35]. In that case, the coupling affects the solitons only over a short interval of their evolution.

Another possibility, which was discussed earlier for various types of optical media [36,37], is to consider the *spatial-domain* dynamics of optical signals carried by dual-core planar waveguides with short fused segments. Such structures can be molded using polymer materials [38], or built into photonic crystals by means of techniques proposed in Ref. [39]. Similar structures are available in plasmonics [40]. An alternative is to use *virtual* dual-core guiding patterns, written in photorefractive media by means of strong pump beams, on top of which probe beams propagate [41]. In such settings, one can consider both stationary spatial solitons trapped by the fused segment of the coupler, and scattering of incident spatial solitons on one or several fused segments. This is the subject of the present work.

The paper is organized as follows. The model is formulated in Sec. II, where we also indicate that it additionally applies to matter-wave couplers for trapped BEC. Collisions of the incident soliton with a local coupler are studied in Sec. III, by means of systematic simulations and three analytical methods, which are relevant in different parametric regions (quasilinear, fast-soliton, and adiabatic approximations). Stationary and excited states of a soliton trapped by the local coupler are considered in Sec. IV, using the VA in combination with a numerical approach. Shuttle oscillations of a soliton trapped between two separated couplers, and in a finite array of couplers, are studied in Sec. V. The paper is concluded by Sec. VI.

II. THE MODEL

The propagation of electromagnetic waves with amplitudes $u(x,z)$ and $v(x,z)$ along direction z in the dual-core planar nonlinear waveguide, fused along a narrow stripe around $x = 0$, which is approximated by the δ function (see a schematic shape of the fused coupler in Fig. 1), obeys coupled nonlinear Schrödinger (NLS) equations, that can be derived in the scaled form, following the lines of Ref. [42]:

$$i \frac{\partial u}{\partial z} = -\frac{1}{2} \frac{\partial^2 u}{\partial x^2} - |u|^2 u - \delta(x) v, \quad (1)$$

$$i \frac{\partial v}{\partial z} = -\frac{1}{2} \frac{\partial^2 v}{\partial x^2} - |v|^2 v - \delta(x) u. \quad (2)$$

Here the second derivatives represent the paraxial diffraction in the transverse direction (x), and the equations are scaled so as to make the coefficients in front of the nonlinear and coupling terms equal to 1. These equations can be derived from Lagrangian $L = \int_{-\infty}^{+\infty} \mathcal{L} dx$, with density

$$\begin{aligned} \mathcal{L} = & \frac{i}{2} (u^* u_z - u_z^* u) - \frac{1}{2} |u_x|^2 + \frac{1}{2} |u|^4 + \frac{i}{2} (v^* v_z - v_z^* v) \\ & - \frac{1}{2} |v_x|^2 + \frac{1}{2} |v|^4 + \delta(x) (u^* v + v^* u). \end{aligned} \quad (3)$$

To relate the scaled form of the model to physical units, one can follow the standard derivation procedure, starting from the wave equation for the electromagnetic fields in the dual-core waveguide [1,42,43]. Straightforward analysis yields the following relation between length l of the fused segment, which is approximated by the δ functions in Eqs. (1) and (2), the coupling length of the fused waveguide, Z_{coupl} , wavelength λ , and characteristic scale X_0 used for the rescaling (it implies that the characteristic spatial width of solitons in physical units is $\sim X_0$):

$$l \sim \lambda Z_{\text{coupl}} / (2\pi X_0). \quad (4)$$

For relevant values $Z_{\text{coupl}} \sim 1$ mm [42,43] and the typical width of the spatial soliton $X_0 \sim 50$ μm , Eq. (4) demonstrates that the typical length of the fused segment is $l \sim 3\lambda$, which is quite realistic in terms of the experimental fabrication of the couplers [44].

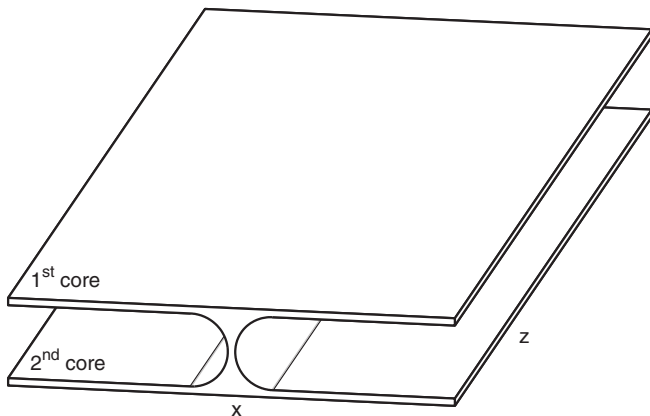


FIG. 1. A schematic structure of the fused planar coupler.

Coupled equations (1) and (2) were simulated using the standard split-step Fourier-transform algorithm, with $\delta(x)$ approximated by a narrow Gaussian, $\hat{\delta}(x)$, which is subject to the normalization condition, $\int_{-\infty}^{+\infty} \hat{\delta}(x) dx = 1$. The width of the regularized δ function was chosen to be essentially smaller than the width of the solitons considered below. We have checked that, under this condition, results of the simulations practically do not depend on the regularization width.

A pair of two locally fused couplers, separated by distance D , is described by the NLS equations with the δ functions multiplied by 1/2, hence the system with $D = 0$ goes over back into Eqs. (1) and (2):

$$i \frac{\partial u}{\partial z} = -\frac{1}{2} \frac{\partial^2 u}{\partial x^2} - |u|^2 u - \frac{1}{2} \left[\delta\left(x - \frac{D}{2}\right) + \delta\left(x + \frac{D}{2}\right) \right] v, \quad (5)$$

$$i \frac{\partial v}{\partial z} = -\frac{1}{2} \frac{\partial^2 v}{\partial x^2} - |v|^2 v - \frac{1}{2} \left[\delta\left(x - \frac{D}{2}\right) + \delta\left(x + \frac{D}{2}\right) \right] u. \quad (6)$$

Further, an array built of $2N + 1$ couplers is described by the extension of Eqs. (5) and (6) with

$$\frac{1}{2} \left[\delta\left(x - \frac{D}{2}\right) + \delta\left(x + \frac{D}{2}\right) \right] \rightarrow C \sum_{n=-N}^N \delta(x - nD), \quad (7)$$

where C is a coupling constant. For solitons whose width is much larger than the array's spacing, D , the comb structure in Eq. (7) may be approximated by a uniform coupling constant, $\bar{C} \equiv C/D$, which acts inside the corresponding box,

$$|x| \leq X_{\text{box}} \equiv ND. \quad (8)$$

It is relevant to mention that Eqs. (1), (2), (5), and (6), with z replaced by time t , are also meaningful as Gross-Pitaevskii equations (GPEs) for BEC loaded into parallel cigar-shaped traps, i.e., matter-wave couplers [18,19]. In that case, the localized coupling may be induced by a transverse laser beam [45]. Analyzing the derivation starting from the underlying three-dimensional GPE [46], it is straightforward to arrive at a relation between the length of the fused area (l), characteristic scale X_0 (which, as well as in the case of the optical system, determines the spatial size of the corresponding matter-wave solitons), and radius a_{\perp} of the transverse confinement of the BEC in the quasi-one-dimensional trap, all taken in physical units:

$$l \sim a_{\perp}^2 / X_0 \quad (9)$$

[cf. Eq. (4)]. For typical values $a_{\perp} \sim 3$ μm and $X_0 \sim 10$ μm [47], Eq. (9) yields $l \sim 1$ μm , which is a relevant estimate for the size of the area induced by a focused laser beam.

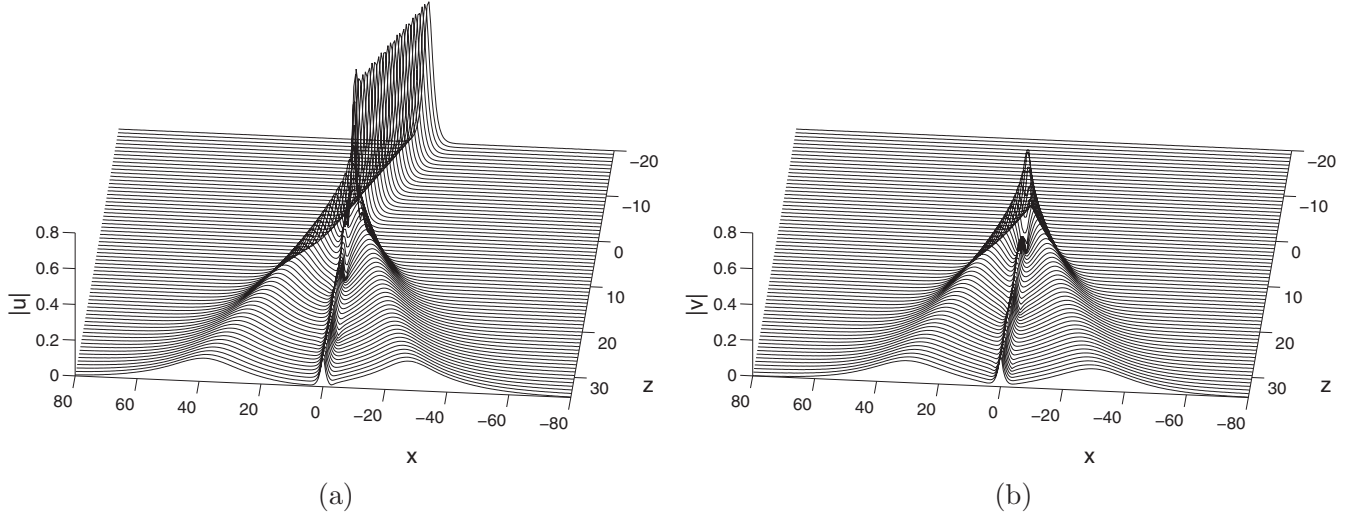


FIG. 2. Collision of an incident soliton with the fused coupler, for $\eta = 0.8$ and $q = 1$ [see Eq. (10)], in the straight (a) and cross (b) cores.

III. COLLISIONS OF THE SOLITON WITH THE SINGLE COUPLER

A. Numerical results

The collision of the incident soliton, launched in the *straight* (u) core, with the local coupler was simulated using Eqs. (1) and (2) with the regularized δ function and the following initial conditions:

$$u(x)|_{z=0} = \eta \operatorname{sech}[\eta(x - \xi_0)] \exp(iqx), v(x)|_{z=0} = 0. \quad (10)$$

Here η is the amplitude of the soliton, q is its velocity [in fact, the tilt of the spatial soliton in the (x, z) plane], and $\xi_0 < 0$ with large $|\xi_0| \gg 1/\eta$ is the initial position. The total power of the incident soliton is $P \equiv \int_{-\infty}^{+\infty} [|u(x)|^2 + |v(x)|^2] dx = 2\eta$.

As shown in Fig. 2, the soliton-coupler interaction gives rise to five waves: transferred (u_T) and reflected (u_R) ones in the straight core; their counterparts, v_T and v_R , in the *cross* (second) core; and a trapped mode oscillating between the two cores in a vicinity of $x = 0$. Obviously, powers of these waves must obey the conservation relation:

$$P(u_T) + P(u_R) + P(v_T) + P(v_R) + P_{\text{trap}} = 2\eta. \quad (11)$$

Results of systematic simulations are summarized in Fig. 3, which demonstrates the splitting of the total power of the incident soliton between the five components. In particular, the power shares carried by the transmitted and reflected waves in the cross core, v_T and v_R , are equal, which is explained below. Panel (d) in this figure demonstrates strong trapping for slowly moving ($q \lesssim 1$) heavy ($\eta \gtrsim 2.5$) incident solitons. At larger velocities, the interaction of the soliton with the local coupler naturally weakens, and the power is chiefly transferred in the straight core, as seen in panel (b). Lighter incident solitons, with $\eta \lesssim 1$, do not generate the trapped mode, being reflected in the straight core at $q \lesssim 0.5$, or transferred to the cross core, where they are evenly split into the transmitted and reflected components, at $q \gtrsim 0.5$. For heavy solitons, with $\eta \gtrsim 3$, panels (b) and (d) exhibit a threshold value of the velocity,

q_{thr} , which is a sharp boundary between the trapping at $q < q_{\text{thr}}$ and transmission at $q > q_{\text{thr}}$.

B. The quasilinear approximation

The nonlinearity in Eqs. (1) and (2) may be neglected in comparison with the coupling terms if the potential energy of the nonlinear self-interaction is much smaller than the intercore coupling energy, which in the present notation implies $\eta \ll 1$. Then, the substitution of $\{u(x, z), v(x, z)\} = \exp(ikz)\{U(x), V(x)\}$, with propagation constant k , into the linearized version of Eqs. (1) and (2) leads to the scattering problem based on the stationary equations,

$$k\{U, V\} = \frac{1}{2} \frac{d^2}{dx^2} \{U, V\} + \delta(x)\{V, U\}. \quad (12)$$

A solution to these equations, with wave number q [cf. Eq. (10)] and the respective value of the propagation constant,

$$k = -q^2/2, \quad (13)$$

is sought for as

$$U(x) = \begin{cases} U_I \exp(iqx) + U_R \exp(-iqx), & x < 0 \\ U_T \exp(iqx), & x > 0, \end{cases} \quad (14)$$

$$V(x) = \begin{cases} V_R \exp(-iqx), & x < 0 \\ V_T \exp(iqx), & x > 0. \end{cases} \quad (15)$$

The amplitudes of the incident, transmitted, and reflected waves are related by conditions of the continuity of $U(x)$ and $V(x)$ at $x = 0$, $U_I + U_R = U_T$, $V_R = V_T$. With regard to this relation, the jump of the first derivatives following from integration of Eq. (12) in an infinitesimal vicinity of $x = 0$ yields another pair of equations for the scattering amplitude, which amount to the form of $V_T = iq^{-1}U_T = -iqU_R$.

A trapped mode may also be generated by Eq. (12): $U = V = U_0 \exp(-|x|)$, where U_0 is an arbitrary amplitude, and the corresponding propagation constant is $k_{\text{trap}} = 1/2$. Because it is separated from values (13), the trapped mode gives no contribution to the linear scattering problem.

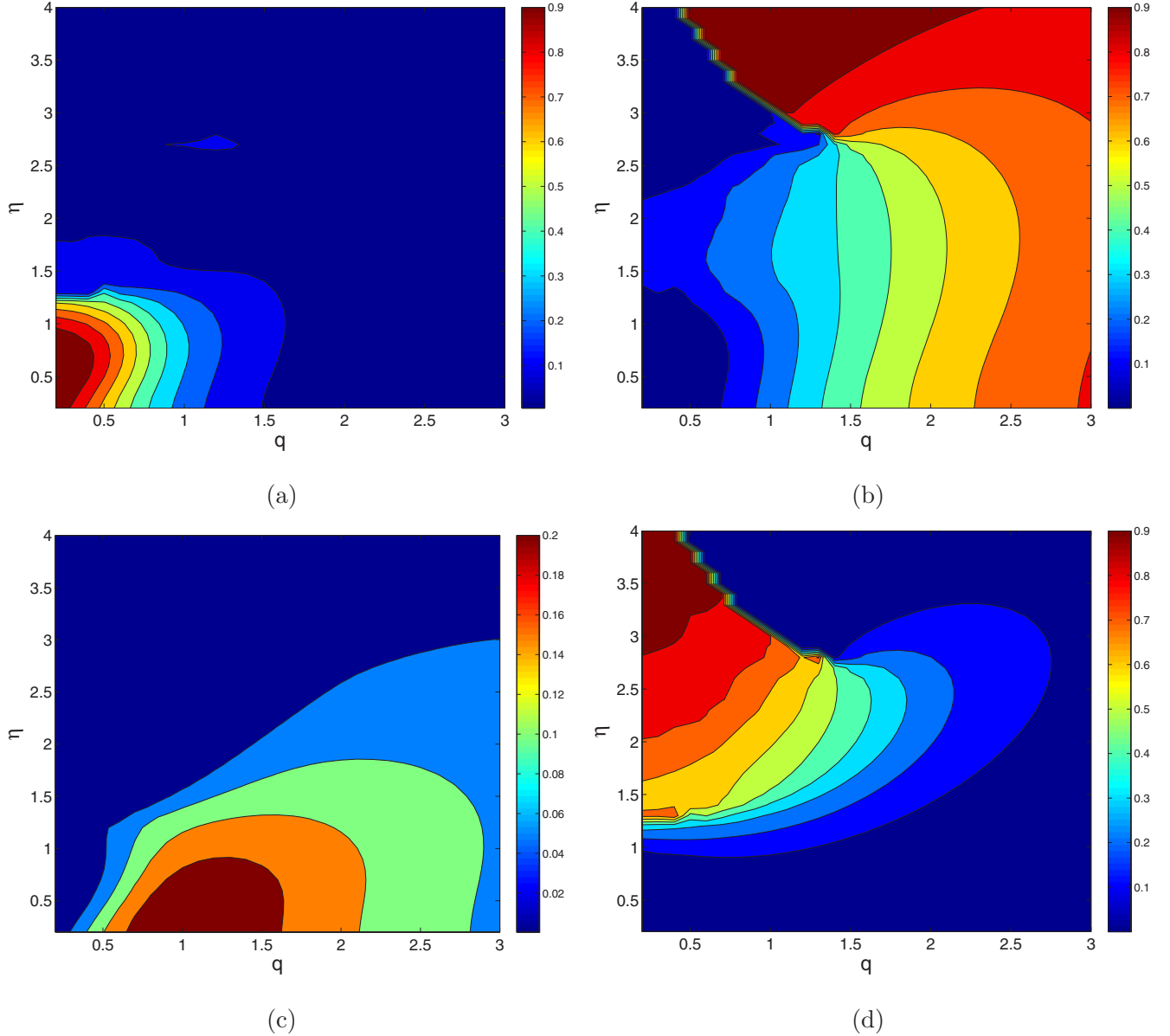


FIG. 3. (Color online) Fractions of the power of the incident soliton reflected (a) and transmitted (b) in the straight core, scattered (transmitted = reflected) in the cross core (c), and trapped by the fused coupler (d), vs the velocity and amplitude of the incident soliton, q and η . The powers obey the balance condition (11).

It is straightforward to find a solution to the continuity and jump equations for the amplitudes:

$$U_R = (q^2 + 1)^{-1} U_I, U_T = -(q^2 + 1)^{-1} q^2 U_I, \quad (16)$$

$$V_R = V_T = -i(q^2 + 1)^{-1} q U_I. \quad (17)$$

This solution satisfies the power-balance condition [see Eq. (11)] and explains the above-mentioned symmetry between the transmitted and reflected waves in the cross core. Further, in Fig. 4 the comparison of the solution, given by Eqs. (16) and (17), to the numerical results for the scattering of the soliton with a sufficiently small amplitude, $\eta = 0.1$, demonstrates a very close agreement between the numerical and analytical results.

C. The interaction of a fast soliton with the local coupler

Another analytical approximation applies to the collision of a fast soliton with the local coupler, when the incident soliton itself remains almost unaffected by the interaction, while generating weak transmitted and reflected waves in the cross core. In the present notation, this case amounts to taking $q \equiv Q \gg 1$ in initial condition (10) [q is replaced here by Q to distinguish it from the wave number in dispersion relation (13)]. The corresponding incident NLS soliton is

$$u = \eta \operatorname{sech}[\eta(x - Qz)] e^{iQx} \exp\left[\frac{1}{2}iz(\eta^2 - Q^2)\right], \quad (18)$$

while Eq. (2) for the cross core may be linearized:

$$i \frac{\partial v}{\partial z} + \frac{1}{2} \frac{\partial^2 v}{\partial x^2} = -\delta(x)u. \quad (19)$$

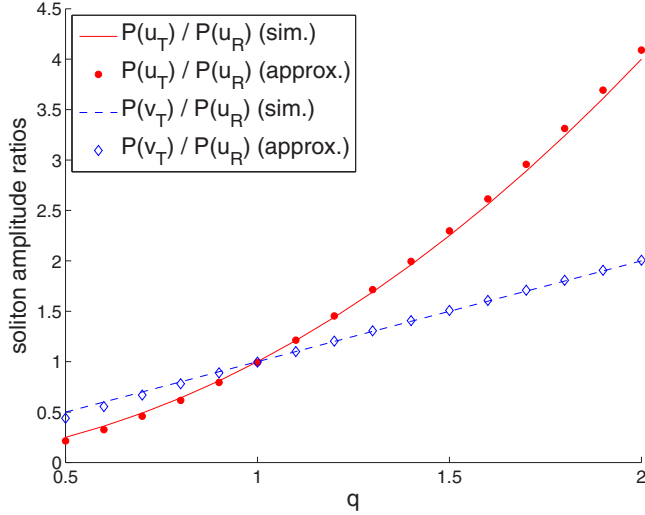


FIG. 4. (Color online) Comparison of the power ratios, given by the analytical solution of the linear scattering problem, as per Eqs. (16) and (17) (curves), to their counterparts produced by direct simulations (chains of symbols) for the small-amplitude soliton with $\eta = 0.1$.

Thus, soliton (18), if substituted in Eq. (19), gives rise to a localized source generating waves in the cross core. As suggested by dispersion relation (13), the source generates two distinct components of solutions, viz., radiation, with $k < 0$, and trapped (nonpropagating) modes with $k > 0$. The so generated wave field can be calculated by means of the Fourier transform. A final result is rather cumbersome, as the emerging integrations cannot be performed analytically. It takes a relatively simple form at $x = 0$, where both radiation and trapped fields have their maxima:

$$\begin{aligned} v_{\text{trap}}(x=0, z) &= -\frac{i}{2Q} \int_0^\infty \sqrt{\frac{2}{k}} \operatorname{sech} \left[\frac{\pi}{2\eta Q} \left(k + \frac{Q^2 - \eta^2}{2} \right) \right] e^{ikz} dk \\ &\approx \frac{[1 - i \operatorname{sgn}(z)] \sqrt{\pi}}{2Q\sqrt{|z|}} \operatorname{sech} \left(\frac{\pi(Q^2 - \eta^2)}{4\eta Q} \right), \end{aligned} \quad (20)$$

$$\begin{aligned} v_{\text{rad}}(x=0, z) &= \frac{i}{2Q} \int_{-\infty}^0 \sqrt{\frac{2}{-k}} \operatorname{sech} \left[\frac{\pi}{2\eta Q} \left(k + \frac{Q^2 - \eta^2}{2} \right) \right] e^{ikz} dk \\ &\approx \frac{[1 + i \operatorname{sgn}(z)] \sqrt{\pi}}{2Q\sqrt{z}} \operatorname{sech} \left(\frac{\pi(Q^2 - \eta^2)}{4\eta Q} \right). \end{aligned} \quad (21)$$

The asymptotic approximations in Eqs. (20) and (21) are valid for $|z| \gg (\eta Q)^{-1}$. Because the present situation is actually considered for large Q and large η , the latter approximations are always relevant, as a matter of fact.

This prediction is compared to results of direct simulations in Fig. 5, where a close agreement is seen. At much larger values of z , the trapped radiation does not follow the asymptotic behavior predicted by Eq. (20), as a broad soliton eventually self-traps in the cross core.

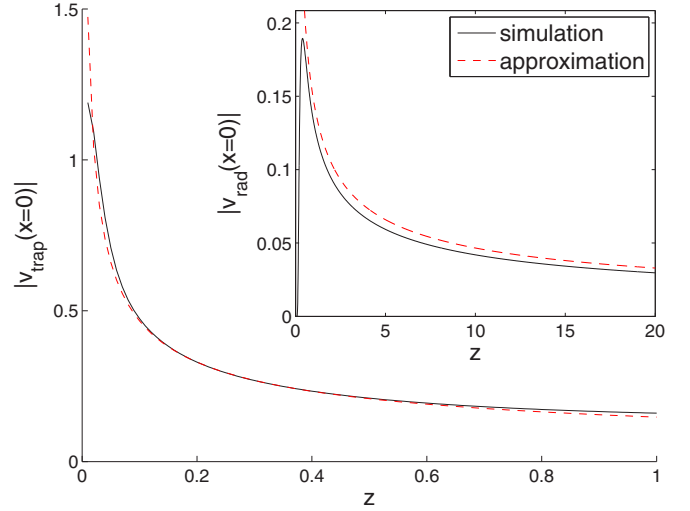


FIG. 5. (Color online) Comparison of the analytical results, given by Eqs. (20) and (21), to their numerical counterparts for the absolute values of the trapped (main plot) and radiation (inset) components of the field in the cross core at $x = 0$, produced by the passage of a fast heavy soliton (18), with $Q = 8$, $\eta = 10$, through the local coupler. The comparison is shown for $z > 0$, as at $z < 0$ (before the soliton passes the fused coupler) it is difficult to separate the numerically generated field into the radiation and trapped components.

D. The adiabatic approximation

In addition to the collision of fast incident solitons with the local coupler, analytically tractable is also the case of a relatively slow heavy soliton, with large η and $q \ll \eta$ in Eq. (10). Accordingly, the soliton moving in the straight core is similar to the one given by Eq. (18),

$$u = \eta \operatorname{sech} \{ \eta [x - \xi(z)] \} \exp(i\xi'x) \exp\left(\frac{1}{2}iz\Lambda\right), \quad (22)$$

where $\xi' \equiv d\xi/dz$ and $\Lambda \equiv (\eta^2 - \xi'^2)$. Further, the field equation in the cross core may be linearized as in Eq. (19) and, accordingly, the solution component in this core, driven by the soliton's field (22) via the local coupler, is easily found in the adiabatic approximation, which treats $\xi(z)$ as a relatively slowly varying function, and omits ξ'^2 in comparison with η^2 :

$$v(x, z) = \exp(i\eta^2 z/2) \operatorname{sech} [\eta\xi(z)] \exp(-\eta|x|). \quad (23)$$

The comparison with direct simulations, displayed in Fig. 6, demonstrates that the amplitude and shape of expression (23) are very close to those of the v component of the numerical solution up to the point of $\xi(z) = 0$, where the incident soliton hits the local coupler. Afterwards, a deviation emerges because the v component does not completely vanish, as is formally predicted by Eq. (23) at $\xi(z) \rightarrow \infty$.

Two terms in Lagrangian density (3) contribute to the interaction between the incident soliton and the local coupler. First, the coupling term generates the attraction potential,

$$W_{\text{coupl}} \equiv - \int_{-\infty}^{+\infty} \delta(x) (u^*v + v^*u) dx = -2\eta \operatorname{sech}^2(\eta\xi), \quad (24)$$

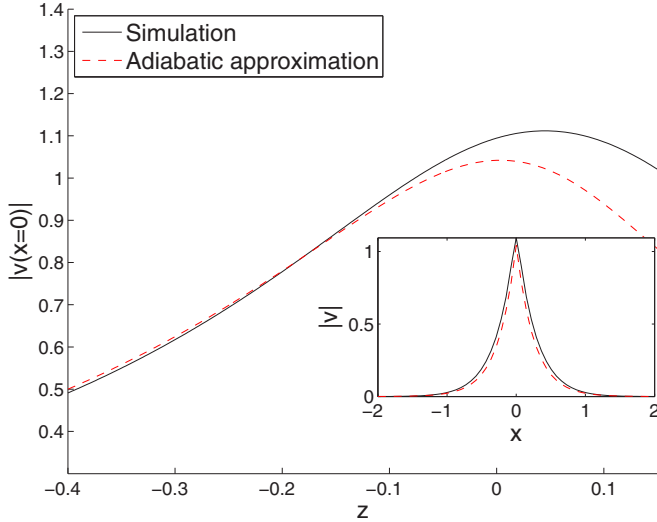


FIG. 6. (Color online) The comparison of the amplitude of the v component of the soliton, predicted by Eq. (23) in the adiabatic approximation, to its counterpart produced by direct simulations, for amplitude $\eta = 4$ and initial velocity $q = 0.456$. The inset shows the comparison of full profiles of the v component at $z = 0$, when the soliton is passing the local coupler.

where use was made of Eqs. (22) and (23). Second, the gradient energy of component (23) gives rise to an effective repulsive potential, $W_{\text{grad}} \equiv \frac{1}{2} \int_{-\infty}^{+\infty} |v_x|^2 dx = \frac{1}{2} \eta \text{sech}^2(\eta\xi)$. Thus, the net potential of the interaction of the soliton with the local coupler is attractive:

$$W_{\text{tot}}(\xi) \equiv W_{\text{coupl}} + W_{\text{grad}} = -\frac{3}{2} \eta \text{sech}^2(\eta\xi). \quad (25)$$

The incident soliton accelerates under the action of this attraction force and attains the largest velocity while passing the local coupler ($\xi = 0$). In the case of a small initial velocity, $q^2 \ll 1$ [see Eq. (10)], the velocity of the heavy soliton passing the coupler is thus predicted by the energy-balance condition, $(M/2)(\xi'_{\text{max}})^2 = -W_{\text{tot}}(\xi = 0)$, where the soliton's mass is $M = 2\eta$. Thus, Eq. (25) predicts $\xi'_{\text{max}} = \sqrt{3}/2$. The prediction is in agreement with direct simulations, which demonstrate that this velocity ranges between 1.1 and 1.2.

In the adiabatic approximation, the reflection of the soliton from the local coupler, which is represented by the potential well given by Eq. (25), cannot be explained, although a reflection area is clearly present in Fig. 3 at $\eta \lesssim 1$, $q \lesssim 0.3$, and an example of periodic reflections is displayed below in Fig. 12 for $\eta = 0.6$, $q = 0.4$ (in those cases, the adiabatic approximation is not relevant, as η is too small). Actually, it is known that *reflection* of solitons from *attractive* potentials is possible beyond the framework of the adiabatic approximation, if the interaction of the soliton with the trapped mode and radiation waves is taken into regard [48].

IV. STATIONARY AND EXCITED MODES TRAPPED BY THE LOCAL COUPLER

A. The stationary modes

Analytical trapped-mode (soliton) solutions to stationary equations (12) with $k > 0$, which also include the nonlinear

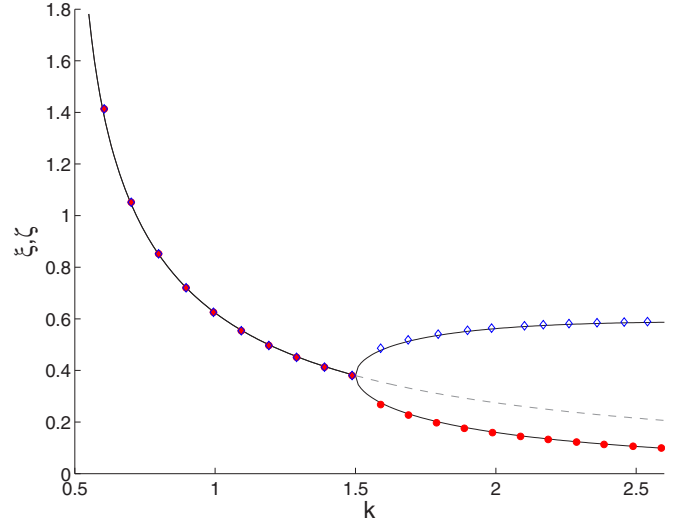


FIG. 7. (Color online) Exact stationary solutions for the symmetric and asymmetric trapped modes, as given by Eqs. (26) and (27), are represented by continuous curves. Numerically found counterparts of these solutions are shown by chains of symbols [the respective values of ξ and ζ are identified via $U(x = 0)$ and $V(x = 0)$ as per Eq. (26)]. The dashed line shows the unstable portion of the symmetric-solution family.

terms U^3 and V^3 , were found in Ref. [37], in the form of

$$\{U(x), V(x)\} = \sqrt{2k} \text{sech}[\sqrt{2k}(|x| + \{\xi, \zeta\})]. \quad (26)$$

For the symmetric trapped mode, positive constant $\xi = \zeta$ is determined by equation $\tanh(\sqrt{2k}\xi) = (2k)^{-1/2}$, hence the symmetric mode exists at $k > 1/2$. On the other hand, as said above, the SBB in the nonlinear coupler gives rise to asymmetric solitons, which in the present case happens at $k_{\text{SBB}} = 3/2$, and at $k > 3/2$ there exists a pair of asymmetric solutions, which are mirror images of each other. They are given by Eq. (26) with

$$\text{sech}^2(\sqrt{2k}\{\xi, \zeta\}) = (4k)^{-1}(2k + 1 \pm \sqrt{4k^2 - 4k - 3}). \quad (27)$$

As shown in Ref. [37], this SBB is of the supercritical type, but these analytical predictions were not compared to numerical solutions before, therefore we have done it here (see Fig. 7). Further, the simulations demonstrate that the symmetric solution at $1/2 < k < 3/2$, as well as the asymmetric ones at $k > 3/2$, are stable, while the symmetric solution is unstable at $k > 3/2$, as expected in the case of the supercritical bifurcation [31].

B. The variational approximation for excited modes

In addition to stationary solutions (26) for trapped modes, it is relevant to analyze excited states of such modes. This can be done on the basis of the variational ansatz,

$$u(x, z) = \eta \text{sech}\{\eta[x - \xi(z)]\} \exp[i\phi(z)], \quad (28)$$

$$v(x, z) = \theta \text{sech}\{\theta[x - \zeta(z)]\} \exp[i\psi(z)], \quad (29)$$

where η , θ and ϕ , ψ are (constant) amplitudes and phases of the two components, while ξ and ζ represent excitations in the form of shifts of the components from the central position, $x = 0$.

Evolution equations for the so excited mode can be derived as Newton's equations of motion for two interacting particles corresponding to the u and v components, which is equivalent to the VA [30]. To this end, we note that potential (24) of the coupling between the components yields, in the present case, $W_{\text{coupl}} = -2\eta\theta \operatorname{sech}(\theta\zeta) \operatorname{sech}(\eta\xi) \cos(\phi - \psi)$. The corresponding equations of motion are $M_{\{u,v\}} d^2\{\xi, \zeta\}/dz^2 = -\partial W_{\text{coupl}}/\partial\{\xi, \zeta\}$, where the above-mentioned effective soliton masses are $M_{\{u,v\}} = 2\{\eta, \theta\}$. Thus, the equations take the form of

$$\frac{d^2\xi}{dz^2} = -\eta\theta \frac{\sinh(\eta\xi) \cos(\phi - \psi)}{\cosh^2(\eta\xi) \cosh(\theta\zeta)}, \quad (30)$$

$$\frac{d^2\zeta}{dz^2} = -\eta\theta \frac{\sinh(\theta\zeta) \cos(\phi - \psi)}{\cosh^2(\theta\zeta) \cosh(\eta\xi)}. \quad (31)$$

Linearization of Eqs. (30) and (31) for small oscillations of ξ and ζ reduces to $d^2\xi/dz^2 = -\eta^2\theta\xi$ and $d^2\zeta/dz^2 = -\eta\theta^2\zeta$, hence eigenfrequencies of the small positional oscillations are predicted to be

$$\Omega_1 \approx \eta\sqrt{\theta}, \Omega_2 = \theta\sqrt{\eta}. \quad (32)$$

These predictions were verified by simulations, as shown in Fig. 8. The simulations were run by applying a small kick to either component of the symmetric or asymmetric trapped mode (26). In the asymmetric configuration, the positional oscillations of the lighter component [the one with a smaller amplitude, which corresponds to a smaller frequency in Eq. (32)] exhibit strong attenuation, unlike robust oscillation of the stronger component. Therefore, only one frequency is shown in Fig. 8 for the excited asymmetric mode.

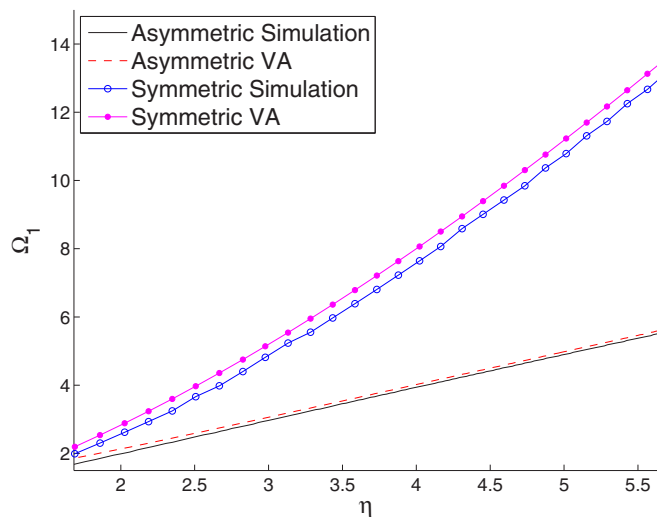


FIG. 8. (Color online) The comparison of the VA prediction for eigenfrequencies of small positional oscillations of the components of the symmetric ($\eta = \theta$, upper lines) and asymmetric ($\eta \neq \theta$, lower lines) trapped modes, as given by Eq. (32), to results extracted from direct simulations.

Small oscillations of the power between the two components (without position shifts) were simulated too. It was found that the respective eigenfrequency is very close to the obvious beating frequency, $\Omega_{12} = (\eta^2 - \theta^2)/2$.

V. PAIRS AND ARRAYS OF LOCAL COUPLERS

A. The interaction of solitons with the double coupler

Simulations of Eqs. (5) and (6) for the collision of an incident soliton with the double locally fused coupler were run using initial condition (10) with amplitude $\eta = 1$, while both the initial velocity q and distance D between the two local couplers were varied. Results of the simulations, summarized in Fig. 9, show a conspicuous correlation between u_R and v_T , i.e., the reflected and transmitted waves in the straight and cross cores, respectively. Similarly, a correlation is observed between the waves transmitted in the straight core, u_T , and reflected in the cross core, v_R . It is worthy to note that the second coupler strongly affects the scattering in the cross core, breaking the symmetry between the transmitted and reflected waves in favor of the latter one, in comparison with the single coupler [cf. Figs. 9(c) and 3(c)]. The share of the power of the incident soliton trapped by the pair of local couplers, which is shown in Fig. 9(d), was evaluated long enough after the incident soliton hit the first local coupler, viz., at $z = 175/q$ (recall q is the incident soliton's velocity). At relatively small velocities, the trapped share increases in comparison with the single coupler ($D = 0$).

The increase of the amplitude of the incident soliton to $\eta = 2$ significantly reduces the portion of the power transferred to the cross core, as evident in Fig. 10 [in particular, in panel (c)]. In this case, a dominant share of the incident power is either trapped or transmitted in the straight core. Accordingly, panels (b) and (d) reveal the presence of a threshold value of the distance between the two couplers, $D_{\text{thr}} \approx 0.6$, which is a sharp boundary between the trapping for $D < D_{\text{thr}}$ and transmission for $D > D_{\text{thr}}$, at $q \lesssim 1.2$. Note that such a threshold is not observed for $\eta = 1$ (cf. Fig. 9).

If the two couplers are set close enough to each other ($D < 0.6$), higher incident powers give rise to strongly excited trapped states, in which the power trapped around both couplers swings in unison between the cores. As the couplers are separated farther, the intercore-swinging mode changes to oscillations between the couplers, while the trapped power is greatly reduced, giving way to a higher power-transmission share in the straight core.

If the distance between the couplers, D , is quite small, the field is trapped in an almost uniform state between them, as shown in Fig. 11. In this case a solution to the stationary version of Eqs. (5) and (6) outside of the couplers (at $|x| > D/2$) has the same form as given by Eqs. (26) and (27), for the symmetric ($U = V$) and asymmetric ($U \neq V$) states alike, while an exact solution between the couplers, at $|x| < D/2$, can be expressed in terms of elliptic functions. Actually, for small D the inner solution for the symmetric state can be approximated by a simple expression which is quadratic in x :

$$U(|x| < D/2) \approx \sqrt{2k-1} \left\{ 1 + \left[\left(\frac{D}{2} \right)^2 - x^2 \right] (k-1) \right\}, \quad (33)$$

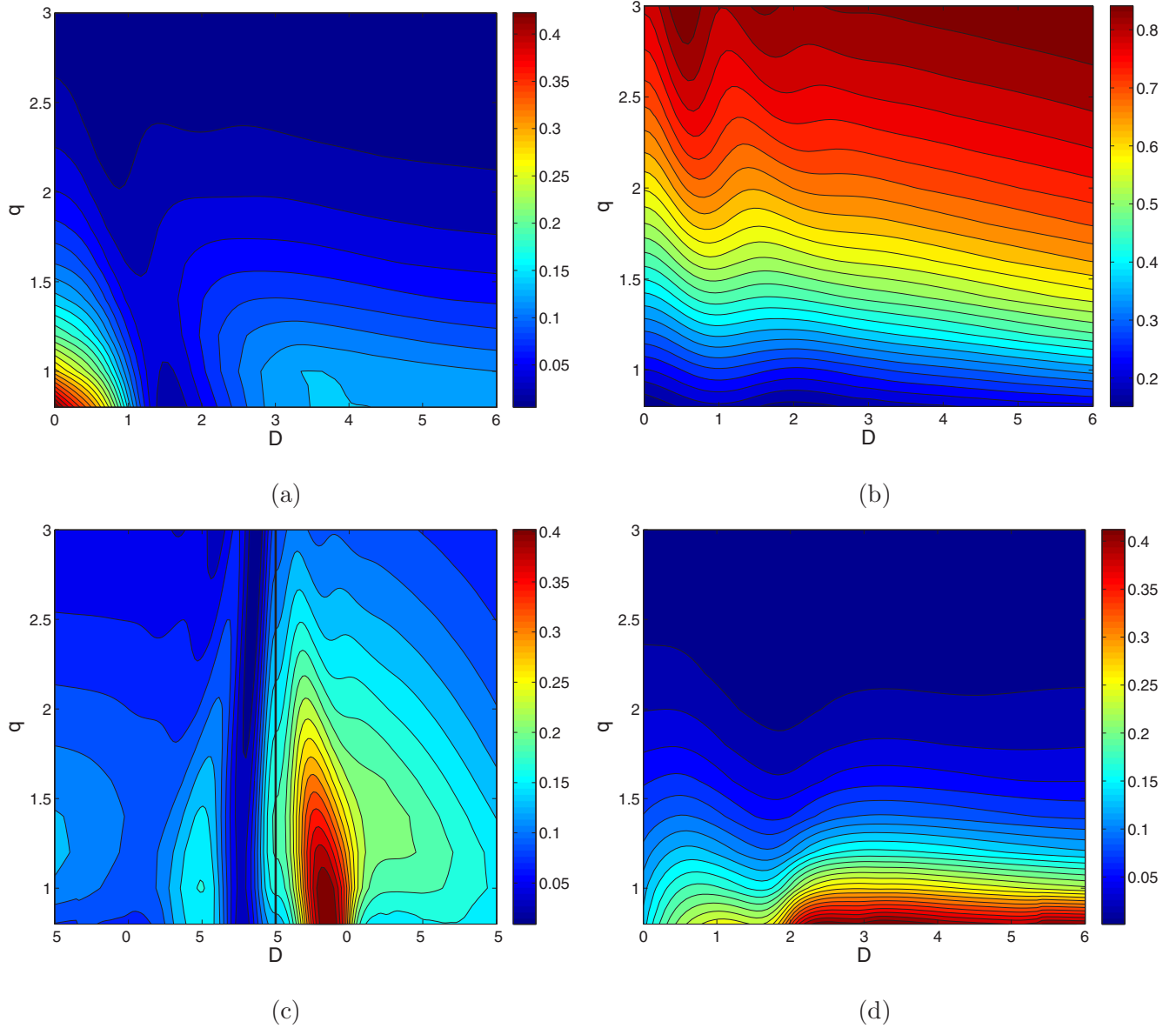


FIG. 9. (Color online) Splitting of the power of the incident soliton, with amplitude $\eta = 1$ and velocity q , hitting the pair of local couplers separated by distance D . (a), (b) Shares of the power reflected and transmitted, respectively, in the straight core. (c) The same for the cross core. In (c), the plots for the reflected and transmitted shares are butt joined to corroborate the equality of these shares for the single coupler ($D = 0$). (d) The trapped-power share.

and similarly for the asymmetric state. Solution (33) explains weak curvature of the intrinsic-layer field observed in Fig. 11.

It is relevant to mention that the dual coupler may give rise to *double symmetry breaking*, combining the SBB of the linearly coupled components, like in Eqs. (26) and (27), and spontaneous breaking of the spatial symmetry between the two local couplers, similar to the well-known symmetry-breaking

effect in double-well potentials [19,49]. Analysis of this problem will be presented elsewhere.

It is relevant to mention too that, for $\sqrt{2k}D \gg 1$, the asymmetric states supported by each local coupler, which are given by Eqs. (26) and (27), can be combined into four different species of composite states trapped by the pair of far separated couplers:

$$\{U(x), V(x)\} = \sqrt{2k} \begin{cases} \{\Psi(|x + \frac{D}{2}| + \xi), \Psi(|x + \frac{D}{2}| + \zeta)\} + \{\Psi(|x - \frac{D}{2}| + \zeta), \Psi(|x - \frac{D}{2}| + \xi)\} \\ \{\Psi(|x + \frac{D}{2}| + \xi), \Psi(|x + \frac{D}{2}| + \zeta)\} - \{\Psi(|x - \frac{D}{2}| + \zeta), \Psi(|x - \frac{D}{2}| + \xi)\} \\ \{\Psi(|x + \frac{D}{2}| + \xi), \Psi(|x + \frac{D}{2}| + \zeta)\} + \{\Psi(|x - \frac{D}{2}| + \xi), \Psi(|x - \frac{D}{2}| + \zeta)\} \\ \{\Psi(|x + \frac{D}{2}| + \xi), \Psi(|x + \frac{D}{2}| + \zeta)\} - \{\Psi(|x - \frac{D}{2}| + \xi), \Psi(|x - \frac{D}{2}| + \zeta)\} \end{cases}, \quad (34)$$

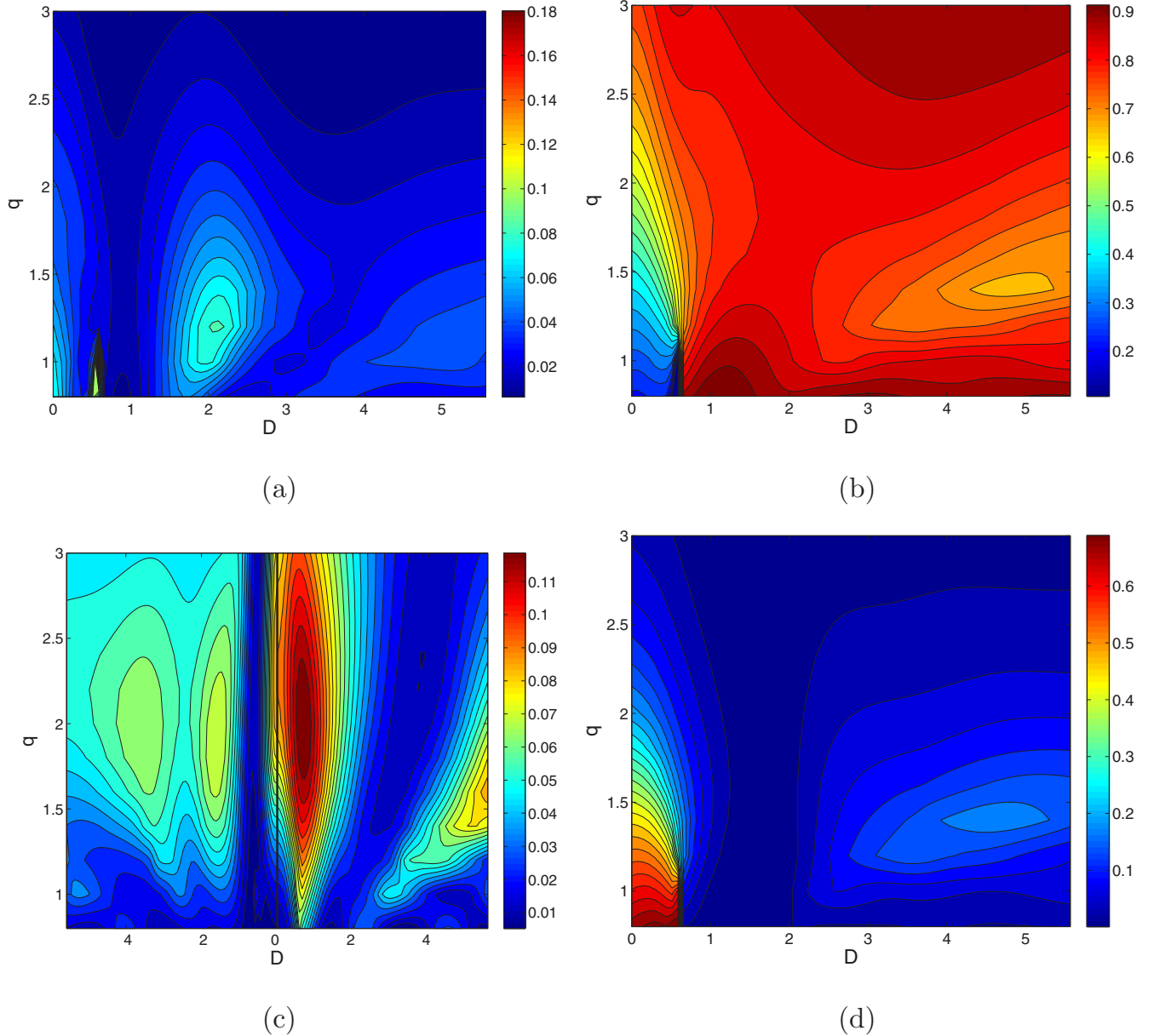


FIG. 10. (Color online) Splitting of the power of the incident soliton, with amplitude $\eta = 2$ and velocity q , which hits the pair of local couplers separated by distance D . (a), (b) Shares of the power reflected and transmitted in the straight core. (c) The same for the cross core. In (c), the plots for the reflected and transmitted shares are butt joined to corroborate the equality of these shares for the single coupler ($D = 0$). (d) The trapped-power share.

where $\Psi(X) \equiv \text{sech}(\sqrt{2k}X)$, while ξ and ζ are given by Eq. (27) with + and -, respectively (hence one has $0 < \xi < \zeta$). The two top lines of Eq. (34) represent, respectively, in-phase and π -out-of-phase *skew composite states*, with the opposite sense of the spontaneous symmetry breaking at the two local couplers: $U(x = -\frac{D}{2}) > V(x = -\frac{D}{2})$ and $|U(x = \frac{D}{2})| < |V(x = \frac{D}{2})|$ (the π phase shift implies opposite overall signs of the fields at $x = \pm\frac{D}{2}$), while the two bottom lines represent in-phase and π -out-of-phase *straight composite states*, with $U(x = -\frac{D}{2}) > V(x = -\frac{D}{2})$ and $|U(x = \frac{D}{2})| > |V(x = \frac{D}{2})|$. In the inner region, $|x| < \frac{D}{2}$,

decaying tails of the in-phase and out-of-phase states are matched (like it was done, in another context, in Ref. [50]) to the following solutions of the linearized stationary equations, $k\{U, V\} = \frac{1}{2}\{U'', V''\}$ [cf. Eq. (12)]:

$$\{U(x), V(x)\}_{\text{in}} = \{U_0, V_0\} \cosh[\sqrt{2k}(x - \{x_U^{(0)}, x_V^{(0)}\})], \quad (35)$$

$$\{U(x), V(x)\}_{\text{out}} = \{U_0, V_0\} \sinh[\sqrt{2k}(x - \{x_U^{(0)}, x_V^{(0)}\})]. \quad (36)$$

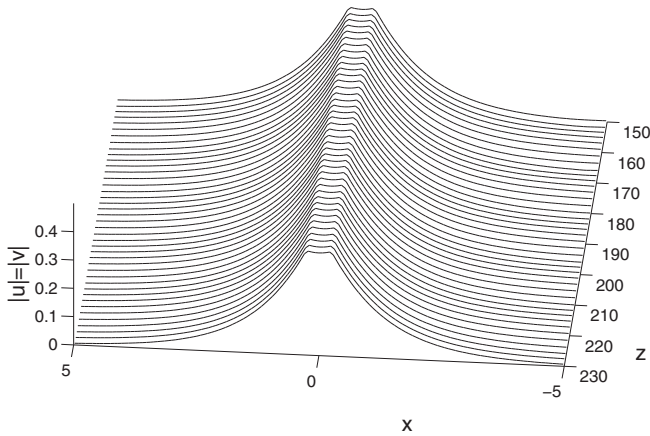


FIG. 11. The wave field in the symmetric state, trapped by the dual coupler of a small width, $D = 0.5$, as a result of the passage of a soliton with amplitude $\eta = 1.0$ and initial velocity $q = 0.8$.

The matching demonstrates that the midpoint of the inner portion of the straight composite modes is not shifted from the system's center, i.e., $x_U^{(0)} = x_V^{(0)} = 0$, while (exponentially small) amplitudes of the respective inner solutions are

$$\{U_0^2, V_0^2\}_{\text{straight}} = 4\sqrt{2k} \exp[-\sqrt{k/2}(D + 2\{\xi, \zeta\})]. \quad (37)$$

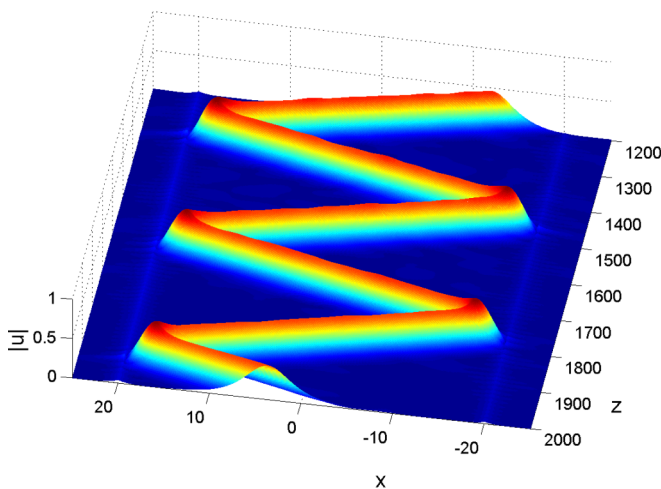
On the other hand, for the skew composite states, the midpoint of each component, $U(x)$ and $V(x)$, is shifted towards the individual soliton with the smaller amplitude in the same component [i.e., with the amplitude corresponding to ζ , rather than ξ , in Eq. (27)]:

$$x_U^{(0)} = -x_V^{(0)} = \frac{1}{2}(\zeta - \xi), \quad (38)$$

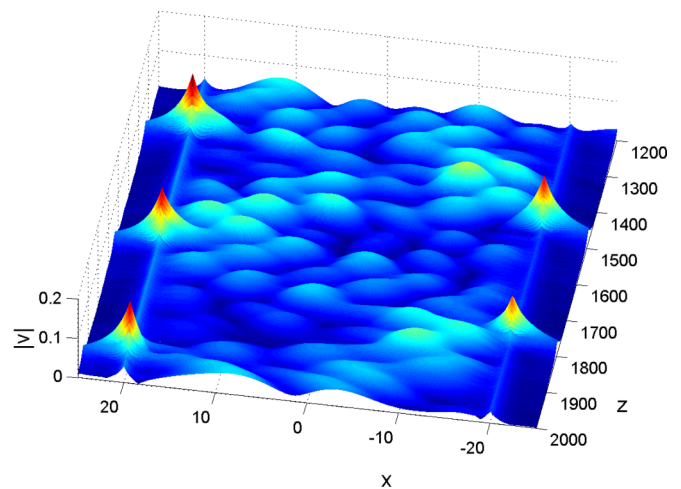
while the corresponding amplitude of the inner solution is

$$(U_0^2)_{\text{skew}} = (V_0^2)_{\text{skew}} = 4\sqrt{2k} \exp[-\sqrt{k/2}(D + \xi + \zeta)]$$

[cf. Eq. (37)].



(a)



(b)

FIG. 12. (Color online) An example of persistent shuttle dynamics of a soliton in a broad cavity ($D = 40$) bounded by two local couplers. The soliton was launched in the u component, with initial amplitude $\eta = 0.6$ and velocity $q = 0.4$. Panels (a) and (b) display absolute values of fields u and v .

Finally, following the lines of Ref. [50], it is possible to compare values of the Hamiltonian of the four species of the composite modes defined in Eq. (34) (the difference in the Hamiltonian is stipulated by the potential of the interaction between the far separated individually trapped solitons): $H_{\text{str}}^{(\text{in})} < H_{\text{skew}}^{(\text{in})} < H_{\text{skew}}^{(\text{out})} < H_{\text{str}}^{(\text{out})}$, hence the straight in-phase state is the ground state, but the other species are expected to be dynamically stable too.

B. Caging a shuttle soliton between two local couplers

The double coupler with large width D can also hold a soliton in the state of shuttle oscillations, similar to soliton-caging cavities formed by pairs of far separated barriers, which occur in other models of nonlinear optics [51]. We describe such a cavity by Eqs. (5) and (6) without factor $1/2$ in front of $[\delta(x - D/2) + \delta(x + D/2)]$, to make each local coupler identical to the solitary one considered above.

A typical example of the persistent shuttle regime in a broad cavity ($D = 40$) is shown in Fig. 12, where a soliton was launched in the u component as per Eq. (10), at $\xi_0 = 0$, with $\eta = 0.6$ and $q = 0.4$. Note that, with these values of the amplitude and velocity, the soliton colliding with the local coupler undergoes a nearly perfect reflection, according to Fig. 3. A dominant share of the soliton's power stays in the straight core, but some power penetrates into the cross core, where it forms a small-amplitude wave pattern whose oscillations are synchronized with the shuttle motion of the strong component of the soliton. Persistent shuttle regimes are also possible for symmetric solitons with equal components.

C. Shuttle oscillations of solitons in multicoupler arrays

An example displayed in Fig. 13 demonstrates that solitons can also be held in the state of persistent shuttle motion in the array defined as per Eq. (7), periodically bouncing from edges of the array. In the example shown in this figure, the

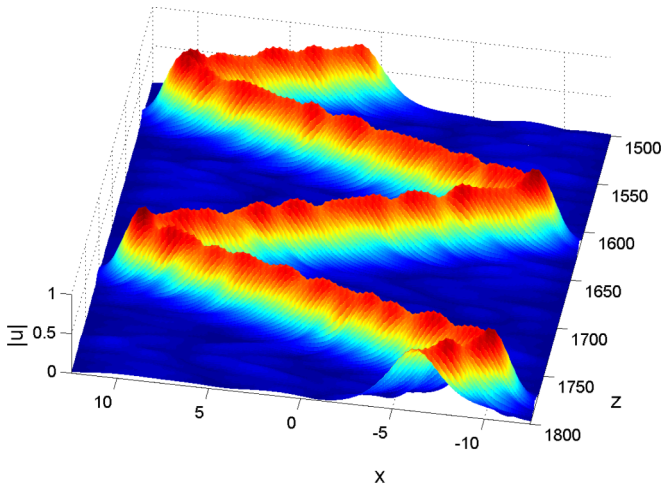


FIG. 13. (Color online) An example of the persistent shuttle motion of a symmetric soliton, created with amplitude $\eta = 1$ and velocity $q = 0.8$, in the array defined as per Eq. (7), with $C = 1/4$ and $D = 0.354$. The number of local couplers in the array is $2N + 1 = 65$. Note that these parameters satisfy the average trapping condition (39).

soliton is symmetric, hence the potential of its interaction with a solitary local coupler is $W_{\text{coupl}}^{(\text{symm})}(\xi) = -2C\eta^2 \text{sech}^2(\eta\xi)$ [see Eq. (24)]. For a broad soliton, with $\eta^{-1} \gg D$, the potentials induced by the comb of couplers can be averaged, making the array tantamount to a potential box of depth $4C\eta/D$ and spatial width $2ND$ [see Eq. (8)]. Thus, the symmetric soliton with the double effective mass, $M^{(\text{symm})} = 4\eta$, is trapped in the box if its squared velocity takes values

$$q^2 < 2C/D. \quad (39)$$

Note that this trapping threshold does not depend on the soliton's amplitude, η .

For strongly asymmetric solitons, with mass $M \approx 2\eta$, the effective potential of the interaction with the solitary coupler is given by Eq. (25), which, in this case, should be here multiplied by C^2 . Thus, the average depth of the respective potential box is $3C^2/D$, and trapping condition (39) is replaced by $q^2 < 3C^2/(D\eta)$, which this time depends on η .

VI. CONCLUSION

The objective of this work is to extend the well-elaborated analysis of the dynamics of solitons in nonlinear couplers to dual-core waveguides fused at one or several narrow segments, which can be approximated by δ functions. The model directly applies to optical spatial solitons in dual-core planar waveguides with the Kerr nonlinearity, as well as to dual traps for the self-attracting BEC. By means of systematic simulations and a combination of several analytical approximations, we have studied collisions of the free soliton with single and double local couplers. The outcome of the collision is characterized by splitting of the total power between five waves, viz., those transmitted and reflected in each core of the waveguide, and the one trapped by the local waveguide. Dynamics of the soliton trapped by the local coupler was studied too, by means of the variational approximation and simulations. Shuttle oscillations of a soliton between two local couplers, and the shuttle motion between edges of a finite array of couplers, were also addressed. In the context of the pair of far separated local couplers, four species of straight and skew trapped two-soliton states were predicted analytically.

The present analysis can be extended in other directions. In particular, it may be interesting, as mentioned above, to study double symmetry breaking in the double local coupler. On the other hand, it may be also relevant to introduce a similar model with the quadratic nonlinearity.

-
- [1] W. P. Huang, *J. Opt. Soc. Am. A* **11**, 963 (1994).
 [2] S. M. Jensen, *IEEE J. Quantum Electron.* **18**, 1580 (1982); A. A. Maier, *Sov. J. Quantum. Electron.* **12**, 1490 (1982).
 [3] S. R. Friberg, Y. Silberberg, M. K. Oliver, M. J. Andrejco, M. A. Saifi, and P. W. Smith, *Appl. Phys. Lett.* **51**, 1135 (1987); D. R. Heatley, E. M. Wright, and G. I. Stegeman, *ibid.* **53**, 172 (1988); W. Królkowski and Y. S. Kivshar, *J. Opt. Soc. Am. B* **13**, 876 (1996); S. C. Tsang, K. S. Chiang, and K. W. Chow, *Opt. Commun.* **229**, 431 (2004); D. Chevriaux, R. Khomeriki, and J. Leon, *Mod. Phys. Lett. B* **20**, 515 (2006).
 [4] I. M. Uzunov, R. Muschall, M. Gölles, Yu. S. Kivshar, B. A. Malomed, and F. Lederer, *Phys. Rev. E* **51**, 2527 (1995).
 [5] F. Lederer, G. I. Stegeman, D. N. Christodoulides, G. Assanto, M. Segev, and Y. Silberberg, *Phys. Rep.* **463**, 1 (2008).
 [6] B. A. Malomed, G. D. Peng, and P. L. Chu, *Opt. Lett.* **21**, 330 (1996).
 [7] H. E. Nistazakis, D. J. Frantzeskakis, J. Atai, B. A. Malomed, N. Efremidis, and K. Hizanidis, *Phys. Rev. E* **65**, 036605 (2002).
 [8] Y. D. Wu, *Fiber Integr. Opt.* **23**, 405 (2004).
 [9] S. Trillo and S. Wabnitz, *J. Opt. Soc. Am. B* **5**, 483 (1988).
 [10] A. Villeneuve, C. C. Yang, P. C. J. Wigley, G. I. Stegeman, J. S. Aitchison, and C. N. Ironside, *Appl. Phys. Lett.* **61**, 147 (1992).
 [11] W. C. K. Mak, B. A. Malomed, and P. L. Chu, *J. Opt. Soc. Am. B* **15**, 1685 (1998).
 [12] Y. J. Tsofe and B. A. Malomed, *Phys. Rev. E* **75**, 056603 (2007); Y. Sun, T. P. White, and A. A. Sukhorukov, *J. Opt. Soc. Am. B* **30**, 736 (2013).
 [13] G. D. Peng, P. L. Chu, and A. Ankiewicz, *Int. J. Nonlin. Opt. Phys.* **3**, 69 (1994).
 [14] W. C. K. Mak, B. A. Malomed, and P. L. Chu, *Phys. Rev. E* **55**, 6134 (1997).
 [15] A. Shapira, N. Voloch-Bloch, B. A. Malomed, and A. Arie, *J. Opt. Soc. Am. B* **28**, 1481 (2011).
 [16] L. Albuch and B. A. Malomed, *Math. Comput. Simul.* **74**, 312 (2007).
 [17] M. Hochberg, T. Baehr-Jones, C. Walker, and A. Scherer, *Opt. Express* **12**, 5481 (2004); J. Petráček, *Appl. Phys. B* **112**, 593 (2013); D. A. Smirnova, A. V. Gorbach, I. V. Iorsh, I. V. Shadrivov, and Y. S. Kivshar, *Phys. Rev. B* **88**, 045443 (2013).

- [18] A. Gubeskys and B. A. Malomed, *Phys. Rev. A* **75**, 063602 (2007); L. Salasnich, B. A. Malomed, and F. Toigo, *ibid.* **81**, 045603 (2010).
- [19] M. Matuszewski, B. A. Malomed, and M. Trippenbach, *Phys. Rev. A* **75**, 063621 (2007).
- [20] G. Herring, P. G. Kevrekidis, B. A. Malomed, R. Carretero-González, and D. J. Frantzeskakis, *Phys. Rev. E* **76**, 066606 (2007); Lj. Hadžievski, G. Gligorić, A. Maluckov, and B. A. Malomed, *Phys. Rev. A* **82**, 033806 (2010); X. Shi, F. Ye, B. Malomed, and X. Chen, *Opt. Lett.* **38**, 1064 (2013).
- [21] X. Shi, B. A. Malomed, F. Ye, and X. Chen, *Phys. Rev. A* **85**, 053839 (2012).
- [22] N. Dror and B. A. Malomed, *Physica D* **240**, 526 (2011).
- [23] R. Driben and B. A. Malomed, *Opt. Lett.* **36**, 4323 (2011); N. V. Alexeeva, I. V. Barashenkov, A. A. Sukhorukov, and Y. S. Kivshar, *Phys. Rev. A* **85**, 063837 (2012); G. Burlak and B. A. Malomed, *Phys. Rev. E* **88**, 062904 (2013).
- [24] A. W. Snyder, D. J. Mitchell, L. Poladian, D. R. Rowland, and Y. Chen, *J. Opt. Soc. Am. B* **8**, 2102 (1991).
- [25] E. M. Wright, G. I. Stegeman, and S. Wabnitz, *Phys. Rev. A* **40**, 4455 (1989).
- [26] C. Paré and M. Florjańczyk, *Phys. Rev. A* **41**, 6287 (1990); A. I. Maimistov, *Sov. J. Quantum. Electron.* **21**, 687 (1991); P. L. Chu, B. A. Malomed, and G. D. Peng, *J. Opt. Soc. Am. B* **10**, 1379 (1993); B. A. Malomed, I. M. Skinner, P. L. Chu, and G. D. Peng, *Phys. Rev. E* **53**, 4084 (1996).
- [27] N. Akhmediev and A. Ankiewicz, *Phys. Rev. Lett.* **70**, 2395 (1993); J. M. Soto-Crespo and N. Akhmediev, *Phys. Rev. E* **48**, 4710 (1993).
- [28] K. S. Chiang, *Opt. Lett.* **20**, 997 (1995).
- [29] M. Romagnoli, S. Trillo, and S. Wabnitz, *Opt. Quantum Electron.* **24**, S1237 (1992).
- [30] B. A. Malomed, *Prog. Opt.* **43**, 71 (2002).
- [31] G. Iooss and D. D. Joseph, *Elementary Stability and Bifurcation Theory* (Springer, Berlin, 1980).
- [32] J. P. Sabini, N. Finalyson, and G. I. Stegeman, *Appl. Phys. Lett.* **55**, 1176 (1989).
- [33] P. L. Chu, Yu. S. Kivshar, B. A. Malomed, G. D. Peng, and M. L. Quiroga-Teixeiro, *J. Opt. Soc. Am. B* **12**, 898 (1995); B. Mandal and A. R. Chowdhury, *Chaos, Solitons Fractals* **24**, 557 (2005).
- [34] V. V. Afanasjev, B. A. Malomed, and P. L. Chu, *Opt. Commun.* **137**, 229 (1997).
- [35] A. Boskovic, S. V. Chernikov, and J. R. Taylor, *J. Mod. Opt.* **42**, 1959 (1995).
- [36] N. Akhmediev and A. Ankiewicz, *Opt. Commun.* **100**, 186 (1993).
- [37] Y. Li, W. Pang, S. Fu, and B. A. Malomed, *Phys. Rev. A* **85**, 053821 (2012).
- [38] L. Eldada and L. W. Shacklette, *IEEE J. Sel. Top. Quant. Electron.* **6**, 54 (2000); H. Ma, A. K. Y. Jen, and L. R. Dalton, *Adv. Mater.* **14**, 1339 (2002).
- [39] M. Bayindir, B. Temelkuran, and E. Ozbay, *Appl. Phys. Lett.* **77**, 3902 (2000); J. R. Salgueiro and Y. S. Kivshar, *Opt. Lett.* **30**, 1858 (2005); S. A. Rinne, F. Garcia-Santamaria, and P. V. Braun, *Nat. Photonics* **2**, 52 (2008).
- [40] L. Liu, Z. H. Han, and S. L. He, *Opt. Express* **13**, 6645 (2005).
- [41] D. Neshev, A. Dreischuh, G. G. Paulus, and H. Walther, *Appl. Phys. B: Lasers Opt.* **72**, 849 (2001); P. G. Kevrekidis, Z. Chen, B. A. Malomed, D. J. Frantzeskakis, and M. I. Weinstein, *Phys. Lett. A* **340**, 275 (2005); Y. V. Kartashov, V. A. Vysloukh, and L. Torner, *Eur. Phys. J.: Spec. Top.* **173**, 87 (2009).
- [42] A. D. Boardman and K. Xie, *Phys. Rev. A* **50**, 1851 (1994).
- [43] G. P. Agrawal, *Nonlinear Fiber Optics*, 4th ed. (Academic, San Diego, 2007).
- [44] A. M. Streltsov and N. F. Borrelli, *Opt. Lett.* **26**, 42 (2001).
- [45] K. Bongs and K. Sengstock, *Rep. Prog. Phys.* **67**, 907 (2004).
- [46] C. J. Pethick and H. Smith, *Bose-Einstein Condensation in Dilute Gases*, 2nd ed. (Cambridge University Press, Cambridge, UK, 2008).
- [47] K. E. Strecker, G. B. Partridge, A. G. Truscott, and R. G. Hulet, *New J. Phys.* **5**, 73 (2003).
- [48] T. Ernst and J. Brand, *Phys. Rev. A* **81**, 033614 (2010).
- [49] G. J. Milburn, J. Corney, E. M. Wright, and D. F. Walls, *Phys. Rev. A* **55**, 4318 (1997); A. Smerzi, S. Fantoni, S. Giovanazzi, and S. R. Shenoy, *Phys. Rev. Lett.* **79**, 4950 (1997); L. D. Carr, Charles W. Clark, and W. P. Reinhardt, *Phys. Rev. A* **62**, 063610 (2000); E. Infeld, P. Ziń, J. Gocalek, and M. Trippenbach, *Phys. Rev. E* **74**, 026610 (2006).
- [50] B. A. Malomed, *Phys. Rev. E* **58**, 7928 (1998).
- [51] P. Y. P. Chen, B. A. Malomed, and P. L. Chu, *Phys. Rev. E* **71**, 066601 (2005); O. Maor, N. Dror, and B. A. Malomed, *Opt. Lett.* **38**, 5454 (2013).